Canard orbits in Fabry-Perot cavities induced by radiation pressure and photothermal effects

F. Marino,[1] M. De Rosa,[2] and F. Marin[3,*]
[1]*INFN, Sezione di Firenze, Via Sansone 1, I-50019 Sesto Fiorentino (FI), Italy*
[2]*CNR-INOA, Sezione di Napoli, Via Campi Flegrei 34, 80078 Pozzuoli (NA), Italy and INFN, Sezione di Firenze, Via Sansone 1, I-50019 Sesto Fiorentino (FI), Italy*
[3]*Dipartimento di Fisica, Università di Firenze, INFN, Sezione di Firenze, and LENS, Via Sansone 1, I-50019 Sesto Fiorentino (FI), Italy*
(Received 15 July 2005; published 22 February 2006)

A theoretical study of a high-finesse Fabry-Perot cavity considering radiation pressure and photothermal displacement is reported. We show that the competition between these two effects induces a different kind of dynamic behavior in such a system, consisting of canard orbits and excitability. The transition between the excitable regime and the canard oscillations, occurring through a supercritical Hopf bifurcation, appears in an order compatible with the van der Pol–FitzHugh-Nagumo equations. Besides its interest as a study of general nonlinear dynamics, the characterization of the effects described is critical for high sensitivity interferometric displacement measurements as those employed for gravitational waves detection.

DOI: 10.1103/PhysRevE.73.026217 PACS number(s): 05.45.−a, 42.65.Sf, 04.80.Nn

I. INTRODUCTION

Periodic oscillations in biological, chemical, and electronic systems have been very frequently observed to be the result of multiple time scale dynamics [1]. The dynamic behavior of systems such as neural cells [2], cardiac tissues [3], chemical reactions [4], among many others [5], can be mathematically described by means of slow and fast variables coupled together (slow-fast systems).

Typical behaviors arising in slow-fast systems are excitability and relaxation oscillations. Excitability was originally described in the field of mathematical biology [5]. Such systems have only one stable steady state but they react to perturbations that overcome a threshold by following a deterministic orbit in phase space which is independent on the details of the applied stimulus. Commonly, systems that exhibit excitability in a particular range of parameters also have a regime of relaxation oscillations. The transition from one type of behavior to the other is described by the theory of bifurcations (Andronov saddle-node collisions, sub- and supercritical Hopf bifurcations, etc.). However, the transitional regime exhibits special features whose physical implications are still the subject of intense studies [6,7]. One of the most popular models describing excitability and relaxation oscillations is the van der Pol–FitzHugh-Nagumo (vdPFN) [8], originally conceived to simply model the neural activity. It can be formalized by the coupled equations

$$\dot{x} = y + x - \frac{x^3}{3}, \tag{1}$$

$$\dot{y} = -\varepsilon(x - a), \tag{2}$$

where the variables x and y evolve with two very different characteristic time scales whose ratio is the small parameter ε. In this model, the transition from the excitable regime characterized by a single steady-state attractor to an oscillatory regime—where the only attractor is a limit cycle—occurs at the critical parameter values $a=a_c=\pm 1$ through a supercritical Hopf bifurcation. Within a range of order ε around the bifurcation point a_c, the amplitude of the resulting limit cycle grows as $\sqrt{a-a_c}$. However, outside this range both the amplitude and the frequency of the limit cycle abruptly (though continuously) change and the resulting oscillation of the fast variable x consists of square-wave-like pulses. The key point of this dynamics is that, since ε is small, one can separate a slow motion taking place on the critical manifold $y=f(x)=(x^3/3)-x$ and a fast motion running essentially perpendicularly to the y axis. Since the critical manifold is attractive for $|x|>1$ and repulsive for $|x|<1$, in the limit $\varepsilon \to 0$, the trajectories slowly flow along the critical manifold until they arrive at one of the fold points $(x,y)=(\pm 1, \mp \frac{2}{3})$; then they jump to the other attractive branch of $f(x)$, follow it until the other fold point, and repeat the cycle [9]. However, if ε is small but finite, after the fold point the trajectories do not jump immediately from one stable branch to the other, but they follow the repelling part of the slow manifold for some time (canard oscillations) [10].

Excitability and relaxation oscillations are typically found in biological and chemical systems. Recently, however, considerable theoretical and experimental efforts have been devoted to find analogies with nonlinear phenomena in optics and physics (pattern formation, solitons, chaos…). In particular, excitability and relaxation oscillations have been shown in semiconductor lasers with optical feedback [11] and semiconductor optical amplifiers [12,13], demonstrating their general interest and opening possibilities of applications such as all-optical generation of pulse trains [14] and pulse reshaping [15].

In this work we study the dynamic behavior of a high-finesse Fabry-Perot cavity considering radiation pressure and the thermal expansion of the mirrors due to the absorbed intracavity light (photothermal effect) [16]. The analysis of these phenomena is of critical importance for extremely sensitive interferometric displacement measurements, including,

*Corresponding author. Electronic address: marin@fi.infn.it

e.g., quantum optics experiments [17,18] and gravitational wave detection. Several studies on the stability of Fabry-Perot cavities in the presence of either radiation pressure [19,20] or photothermal expansion [21] have been developed, focused on large baseline gravitational wave detectors.

Previous experimental and theoretical works on high finesse Fabry-Perot cavities have shown the existence of a bistable regime induced either by radiation pressure [22,23] or by photothermal effect [24]. Here we show that, when considered together, these effects can produce a substantially different nonlinear behavior consisting of canard orbits and excitability arising in the vicinity of a supercritical Hopf bifurcation. We observe that the dynamic scenario, in particular the transition from the quasiharmonic Hopf limit cycle to the canard oscillations, is compatible with that of the vdPFN model. We finally characterize the canard regime and the corresponding phase-space trajectories as a function of the system parameters. Since such dynamics are common to a variety of natural systems, the interest of the present study goes beyond the domain of nonlinear optics.

The paper is organized as follows: in Sec. II we discuss the physical mechanism leading to excitability and canard regime in our system. In Secs. III and IV we introduce the physical model and we study the linear stability of its steady state solutions showing the occurrence of a supercritical Hopf bifurcation. In Sec. V we report a numerical study of the model, choosing realistic system parameters. Finally, in Sec. VI we present our conclusions.

II. CANARDS IN THE CAVITY: PHYSICAL MECHANISM

The intracavity field stored in a high-finesse Fabry-Perot interferometer can be orders of magnitude greater than the input field. For a sufficiently high intracavity optical power the radiation-pressure force can significantly change the length of the cavity, thus affecting the intracavity field and hence the radiation pressure itself. This feedback effect leads to a nonlinear intensity dependence of the optical path as in the case of a Kerr medium.

On the other hand, the intracavity field changes the temperature of the mirrors via residual optical absorption. This temperature variation translates into changes of the cavity length through thermal expansion of the mirrors (photothermal effect). This effect clearly depends on the power impinging on the mirrors surface, leading again to an intensity dependent cavity length as for the radiation pressure. If the photothermal effect or the intracavity radiation pressure are sufficiently strong to induce a cavity resonance variation of the order of the Fabry-Perot optical linewidth, the system exhibits a bistable behavior.

We now consider a Fabry-Perot cavity in the presence of both significant radiation pressure and photothermal effects. Let us suppose to inject a monochromatic beam on the long wavelength side with respect to the cold-cavity resonance (i.e., the resonance frequency in absence of radiation pressure and photothermal effects). The radiation pressure, pushing the mirrors, tends to increase the cavity length respect to the cold-cavity value. The cavity resonance moves towards the injected wavelength and therefore the intracavity intensity increases. The intracavity field has the further effect of slowly varying the temperature of the mirrors. Heating induces a decrease of the cavity length through the mirror's thermal expansion, and it moves away the cavity resonance thereby decreasing the intracavity intensity. Under proper conditions the competition between these effects, together with the fact that they operate at different time scales, can lead to self-sustained oscillations and excitability of the optical intensity.

III. DESCRIPTION OF THE MODEL

We consider a Fabry-Perot interferometer with high finesse F and intracavity power P_c. We write the cavity length variations L with respect to its cold-cavity value as $L(t) = L_{rp}(t) + L_{th}(t)$, where L_{rp} and L_{th} are induced respectively by the radiation pressure and the thermal expansion of the mirrors.

In the limit of small displacements, the system composed by the mirrors and the cavity spacer and optical mounts can be sketched as a damped oscillator forced by the intracavity field [23]. Such an assumption is realistic if one mechanical mode of the real system has low resonance frequency and stiffness with respect to the other modes [25]. A typical example is the optomechanical readout system of the gravitational wave detector Auriga [26], where one cavity mirror is fixed on a mechanical oscillator with resonance frequency of about 1 kHz. Well described by this assumption are also large interferometers with suspended mirrors, and microoscillators (MEMS). The evolution equation for L_{rp} reads

$$\ddot{L}_{rp} + \frac{\Omega}{Q}\dot{L}_{rp} + \Omega^2 L_{rp} = \frac{2P_c}{mc}, \tag{3}$$

where Ω is the resonant oscillation frequency, Q is the mechanical quality factor, m is the oscillator effective mass, and c is the light velocity. We are assuming viscous damping for simplicity, but the phenomena described do not change in the case of different (e.g., structural) damping. If λ is the injected field wavelength, the half width at half maximum Δ of the optical spectrum is given by $\Delta = \lambda/4F$. By introducing the dimensionless detuning $\phi = L_{rp}/\Delta$ and time scale $t' = \Omega t$, Eq. (3) becomes

$$\ddot{\phi} + \frac{1}{Q}\dot{\phi} + \phi = \tilde{\alpha} P_c, \tag{4}$$

where $\tilde{\alpha} = 2/mc\Omega^2\Delta$ and from now on the time derivatives are considered with respect to t'.

The other effect of the intracavity field is changing the cavity length through photothermal expansion. A correct calculation of this effect requires the use of three-dimensional thermal diffusion and stress-balance equations [27]. The system is characterized by a typical frequency given by

$$\omega_c = \frac{1}{\tau_c} = \frac{\kappa}{\rho C r_0^2},$$

where κ is the thermal conductivity of the mirror, ρ is its density, C is its specific heat capacity, and r_0 is the beam

radius (assuming a Gaussian transverse profile), defined as the radius at which the power drops to $1/e$ of its central value. A calculation approximating the mirror as an half infinite space shows that the frequency response of the length variations $\delta l(\omega)$, due to a modulated intracavity power $\delta P_c(\omega)$, is given by

$$\delta l(\omega) = BG(\omega/\omega_c)\delta P_c(\omega),$$

where

$$G(\tilde{\omega}) = \frac{1}{\pi}\int_0^\infty du \int_{-\infty}^\infty dv \frac{u^2 e^{-u^2/2}}{(u^2+v^2)(u^2+v^2+i\tilde{\omega})} \tag{5}$$

and B depends on the properties of the mirror material and on the absorption coefficient [28]. Well above ω_c, the frequency response follows an intuitive 1/frequency low as in a standard single-pole system. However, already at $\omega=\omega_c$, the deviation from the single-pole behavior is meaningful and the response has a slow, logarithmic divergence at low frequencies, verified experimentally [16]. The inclusion of finite mirror size effects are necessary to eliminate the divergence and describe the response at very low frequencies (as well as in the stationary state) [29].

On the other hand, the use of the three-dimensional diffusion term in the temporal evolution equations would complicate too much our model, preventing from understanding the main features of the dynamic behavior. Therefore we will adopt a simple single-pole model in our analytical calculations and in most of the numeric work while we will describe some numeric simulations including a realistic photothermal response in Sec. VI, showing that the main features of the dynamics are qualitatively maintained. Hence we assume that the temperature relaxes towards its equilibrium value T_0 at a rate ε, and evolves according to

$$\dot{T} = -\varepsilon\left(T - T_0 - \frac{dT}{dP_c}P_c\right).$$

By linearizing the temperature dependence of L_{th} around the equilibrium we get

$$\dot{L}_{th} = -\varepsilon\left(L_{th} + \left|\frac{dL_{th}}{dP_c}\right| P_c\right), \tag{6}$$

where the positive sign in front of the coefficient $|dL_{th}/dP_c|$ accounts for the shortening of the cavity at increasing mirror temperature. By defining the dimensionless photothermal detuning $\theta=L_{th}/\Delta$, Eq. (6) becomes

$$\dot{\theta} = -\varepsilon(\theta + \tilde{\beta}P_c), \tag{7}$$

where $\tilde{\beta}=|d\theta/dP_c|$ depends on the thermo-optical properties of the mirrors and on the beam waist. Equation (7) is equivalent to the one derived in Ref. [21] starting from a complete thermoelastic model.

Equations (4) and (7) are coupled together through the intracavity power, which depends on the detunings ϕ and θ. Under the assumption that the optical field evolves on a fast time scale as compared to the radiation pressure and thermal effects and then instantaneously follows the cavity length variations (adiabatic approximation), we have

$$P_c = \frac{AP_{in}}{1+\left\{\frac{4F}{\lambda}[L(t)+L_0]\right\}^2}, \tag{8}$$

where P_{in} is the injected power, L_0 is the cold cavity length, and we have assumed that, due to the small displacements induced by the radiation pressure and photothermal effects, the laser wavelength is always close enough to a cavity resonance to keep the Lorentzian approximation of the Fabry-Perot intracavity field. We stress that when the photon lifetime is comparable to the radiation pressure and/or thermal time scales the adiabatic elimination of the optical field is no longer valid. Retardation effects in pendular Fabry-Perot cavities have been previously studied [19] showing that the equilibrium points that are stable if analyzed in the adiabatic approximation can be actually unstable. However, in most cases (see, e.g., Refs. [21,23]) the adiabatic elimination is well justified and it allows us to identify the main physical mechanisms for the canards scenario in this first approach to the problem.

Hence, using the definitions of Δ, ϕ, and θ, the final equations read

$$\ddot{\phi} + \frac{1}{Q}\dot{\phi} + \phi = \alpha P, \tag{9a}$$

$$\dot{\theta} = -\varepsilon(\theta + \beta P), \tag{9b}$$

$$P = \frac{1}{1+(\delta_0+\phi+\theta)^2}, \tag{9c}$$

where $\delta_0=L_0/\Delta$, $\alpha=\tilde{\alpha}AP_{in}$, $\beta=\tilde{\beta}AP_{in}$, and we have defined the adimensional optical power $P=P_c/AP_{in}$.

IV. ANALYTICAL TREATMENT

A. Linear stability analysis

The system is characterized by three real dynamic variables, the radiation-pressure detuning ϕ, its rate of change $\dot{\phi}$, and the photothermal detuning θ:

$$\dot{\phi} = v, \tag{10a}$$

$$\dot{v} + \frac{1}{Q}v = -\phi + \frac{\alpha}{1+(\delta_0+\phi+\theta)^2}, \tag{10b}$$

$$\dot{\theta} = -\varepsilon\left[\theta + \frac{\beta}{1+(\delta_0+\phi+\theta)^2}\right]. \tag{10c}$$

The steady state solutions (v_s, ϕ_s, θ_s) are defined by the implicit cubic equations

$$v_s = 0, \tag{11a}$$

$$-\phi_s[1+(\delta_0+\phi_s+\theta_s)^2] + \alpha = 0, \tag{11b}$$

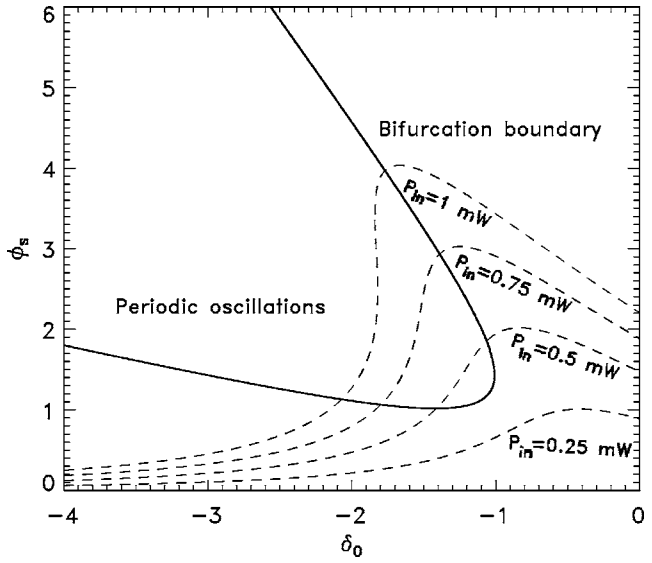

FIG. 1. Boundary of the Hopf bifurcation [Eq. (14)] in the (ϕ_s, δ_0) plane (solid line) and the stationary solutions ϕ_s for different values of the injected power (dashed lines). The parameters are $Q=1$, $\beta=\tilde{\beta}AP_{in}=2.4P_{in}$, $\alpha=\tilde{\alpha}AP_{in}=4P_{in}$ with P_{in} expressed in mW (see the "system parameters" subsection Sec. V A).

$$\theta_s[1+(\delta_0+\phi_s+\theta_s)^2]+\beta=0. \tag{11c}$$

Depending on the values of α, β, and δ_0, the system can have either one or three fixed points. The change in the number of stationary points occurs on the curve

$$\left(\frac{\delta_0^2-3}{9}\right)^3=\left[\frac{(\alpha-\beta)}{2}+\frac{1}{3}\delta_0\left(1+\frac{\delta_0^2}{9}\right)\right]^2, \tag{12}$$

where two steady states coalesce in a saddle-node bifurcation. However, in the present work we restrict our analysis to the case where the system has only one steady state solution.

In order to study the stability of the steady state against small perturbations $(\delta v, \delta\phi, \delta\theta)$, we perform the usual linear stability analysis and we obtain, neglecting the higher order terms and using Eqs. (10a)–(10c), the following coupled equations:

$$\dot{\delta\phi}=\delta v, \tag{13a}$$

$$\dot{\delta v}=-\frac{1}{Q}\delta v-(1+C\phi_s)\delta\phi-C\phi_s\delta\theta, \tag{13b}$$

$$\dot{\delta\theta}=-\varepsilon[C\theta_s\delta\phi+(1+C\theta_s)\delta\theta], \tag{13c}$$

where we call $C=2(\delta_0+\phi_s+\theta_s)/[1+(\delta_0+\phi_s+\theta_s)^2]$. Equations (13a)–(13c) admit nontrivial solutions of the form $\mathbf{K}e^{\Lambda t}$, where $\mathbf{K}$ is an arbitrary column vector, for eigenvalues Λ given by

$$\Lambda^3+a_1\Lambda^2+a_2\Lambda+a_3=0,$$

with coefficients given by

$$a_1=\varepsilon(C\theta_s+1)+\frac{1}{Q},$$

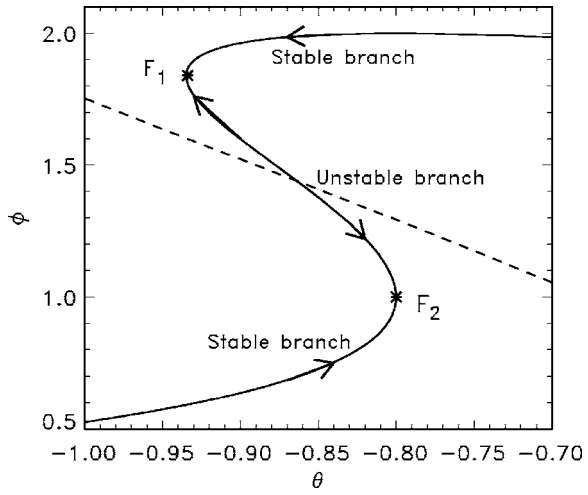

FIG. 2. Slow manifold (solid line) and $G=0$ curve (dashed line) in the (θ, ϕ) space, for $\alpha=2$, $\beta=1.2$ and $\delta_0=-1.2$. The stars indicate the fold points separating the stable and unstable branches of the manifold.

$$a_2=1+C\phi_s+\frac{\varepsilon}{Q}(C\theta_s+1),$$

$$a_3=\varepsilon(C\theta_s+C\phi_s+1).$$

Since $\theta_s=-(\beta/\alpha)\phi_s$ [see Eqs. (10a)–(10c)], one can easily calculate the Hopf stability boundary in the plane (ϕ_s, δ_0). At this purpose we set to zero the real part of the eigenvalue Λ assuming $\Lambda=i\nu$. By replacing this expression in the characteristic equation and separating the real and imaginary parts, we obtain the conditions for the Hopf frequency and the bifurcation boundary

$$\nu^2=a_2,$$

$$a_2a_1-a_3=0. \tag{14}$$

The boundary of the Hopf bifurcation in the (ϕ_s, δ_0) plane is plotted in Fig. 1 (solid line), while the dashed lines represent the steady state solutions ϕ_s for different values of the injected optical power P_{in}. If P_{in} is low enough (0.25 mW in the figure), the fixed point of the system is always stable. However, for sufficiently high injected power levels, the steady state solution loses stability in correspondence of a critical value of δ_0 and a finite-frequency limit cycle starts to grow (supercritical Hopf bifurcation). Further increasing of δ_0 leads to the "inverse" bifurcation and the system passes from the oscillatory dynamics to a new steady state solution. As one can see in Fig. 1, for suitable values of δ_0 the same behavior can be observed in correspondence of different power levels. On the other hand, accordingly with Eq. (12), if P_{in} is larger than a certain value ($\approx$1.2 mW) the oscillatory behavior disappears and the system becomes bistable.

B. Slow manifold and relaxation oscillations

The linear stability analysis provides information about the dynamic behavior only within a small range around the

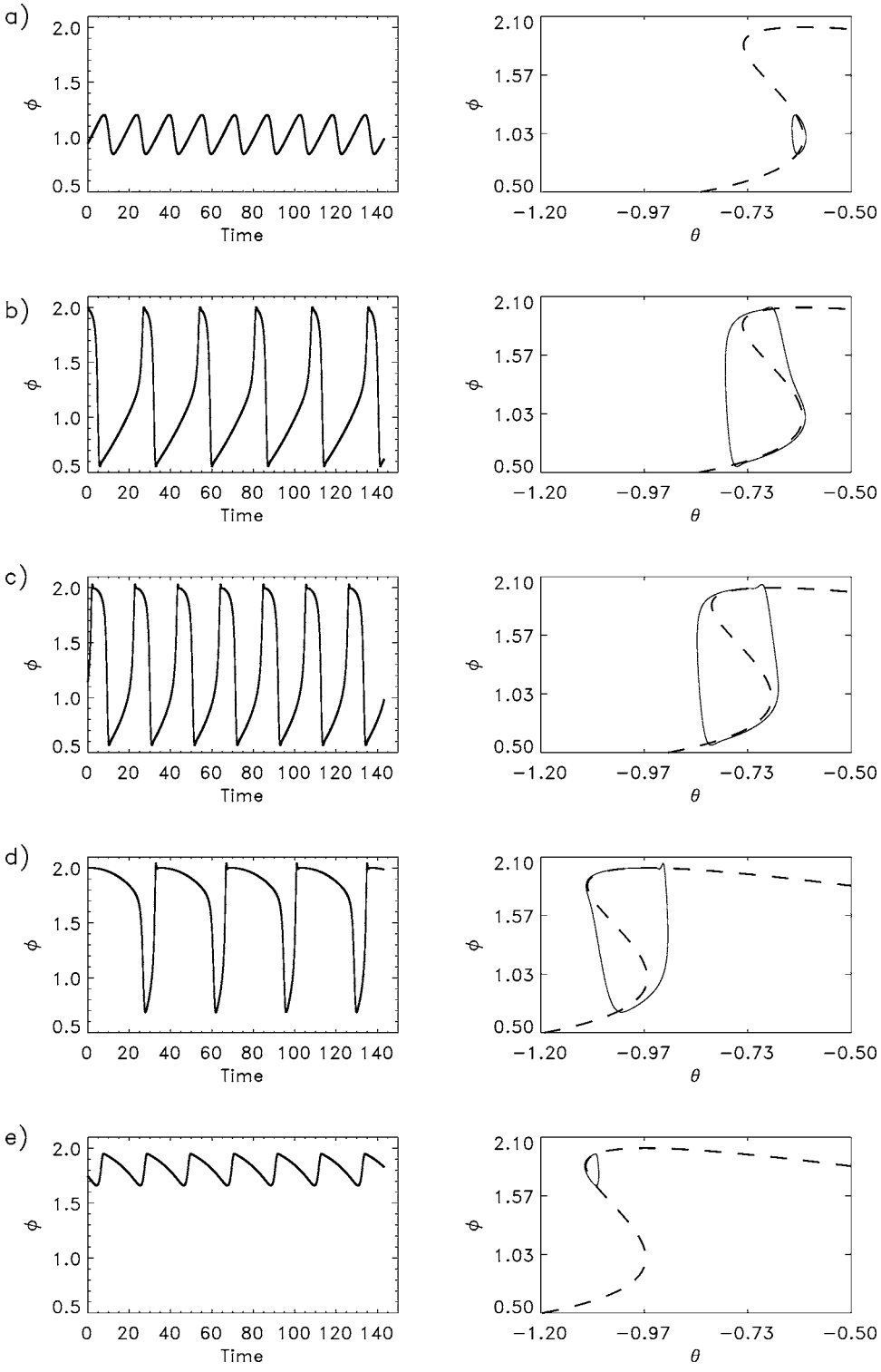

FIG. 3. Temporal evolution of the dynamic variable ϕ and corresponding phase portrait projection (ϕ, θ) compared to the slow manifold (dashed line). The time variable is normalized to the natural period of the mechanical oscillator. (a) $\delta_0=-1.392$, (b) $\delta_0=-1.390$, (c) $\delta_0=-1.320$, (d) $\delta_0=-1.040$ (e), $\delta_0=-1.037$. $P_{in}=0.5$ mW.

bifurcation point, where the system exhibits a small amplitude harmonic limit cycle with frequency ν. However, as we mentioned in the Introduction, beyond this parameter range the periodic solutions of slow-fast systems experience a sudden change both in frequency and amplitude and the resulting oscillation of the fast variable consists of square-wave-like pulses. The blowup of such a limit cycle can be understood by considering the limit $\varepsilon=0$ in Eqs. (10a)–(10c). If $Q^{-1} \gg \varepsilon$, the evolution of θ is slow with respect to that of the other variables and we can analyze separately slow and fast motions. The fast motion follows Eqs. (10a) and (10b) (fast subsystem), where θ is constant and has to be considered as a bifurcation parameter. On the other hand, by introducing the time-scale change $\tau=\varepsilon t$ and putting $\varepsilon=0$, one can see that the slow motion is limited to trajectories evolving accordingly to the slow subsystem equation

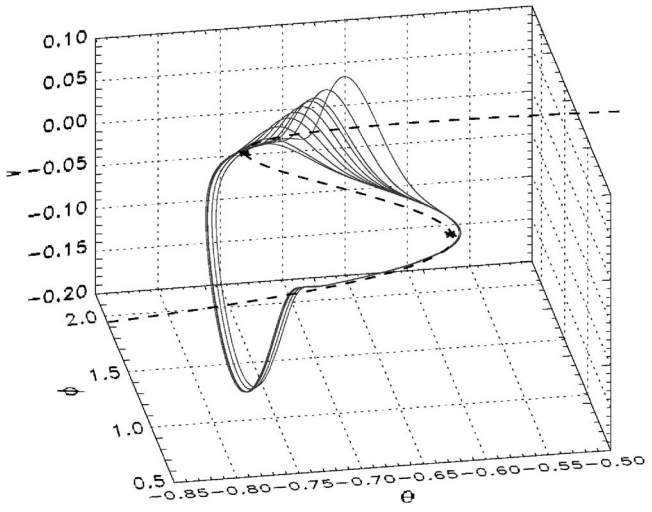

FIG. 4. Canard orbits in the phase space (ϕ,θ,v) compared to the slow manifold (dashed line) as δ_0 is varied (the slow manifold does not change appreciably over the considered range of δ_0). Fold points are indicated by stars. Parameters: $\delta_0=-1.391\,290$, $-1.391\,289$, $-1.391\,288$, $-1.391\,285$, $-1.391\,280$, $-1.391\,270$, $-1.391\,250$, $-1.391\,230$, $-1.391\,215$, $-1.391\,20$; $P_{in}=0.5$ mW.

$$\dot{\theta}=-\left[\theta+\frac{\beta}{1+(\delta_0+\phi+\theta)^2}\right]\equiv G(\phi,\theta) \tag{15}$$

with the constraining conditions $v=0$ and

$$-\phi+\frac{\alpha}{1+(\delta_0+\phi+\theta)^2}\equiv F(\phi,\theta)=0, \tag{16}$$

which implicitly defines a multivalued function $\phi(\theta)$. Hence the set $\Sigma=[(\phi,\theta,v)\in\{v=0\}\cap\{F(\phi,\theta)=0\}]$ (slow manifold), consisting of fixed points of the fast subsystem, defines the branches of slow motions in the phase space. As we will see the dynamics of the complete system can be understood in terms of the respective fast and slow subsystems. By linearizing the fast subsystem evolution equations around points of the set Σ it is simple to see that the equilibria of the fast subsystem are stable if $C\phi>-1$ and unstable if $C\phi<-1$. The boundaries separating the stable branches of the slow manifold from the unstable part (the points $F_{1,2}$ in Fig. 2) are determined by Eq. (16) together with the condition $C\phi=-1$.

We now consider the slow subsystem: from Eqs. (15) and (16) we have that

$$\dot{\theta}=-\left[\theta+\frac{\beta}{\alpha}\phi(\theta)\right]. \tag{17}$$

In Fig. 2 we show in the (θ,ϕ) plane the curves $\phi(\theta)$ and $G=0$ for a fixed value of δ_0. The intersection between these functions, where $\phi(\theta)=-(\alpha/\beta)\theta\equiv p$, is the fixed point of the complete system. From Eq. (17) we see that $\dot{\theta}>(<)0$ if $\phi(\theta)<(>)p$, conditions determining the flow direction on the slow manifold indicated by the arrows in Fig. 2. A trajectory will follow an attracting part of the slow manifold until a fold point where it is pushed out and instantaneously jumps to the other attracting branch of Σ. Then, it flows along this branch until the other fold point where it jumps back, and the system evolves on a limit cycle with a determined natural frequency. On the other hand, for values of δ_0 for which the $G=0$ curve intersects one of the stable branches of the slow manifold, it is immediate to see using the same arguments that the only attractor is a stable fixed point.

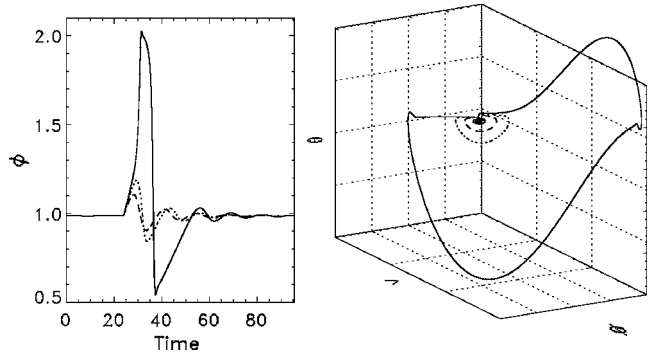

FIG. 5. Responses of the system to a δ-like perturbation of variable amplitude (left) and the corresponding phase-space trajectories (right) when the system is in its stable fixed point ($\delta_0=-1.41$): $x_0=7\times10^{-3}$ (dashed trace), $x_0=8\times10^{-3}$ (dotted trace), $x_0=9\times10^{-3}$ (solid trace). The time variable is normalized to the natural period of the mechanical oscillator. The perturbation is applied at the time $t_0=23$.

We note that the structure and the stability of the slow manifold is analogous to that of Eqs. (1) and (2) which supports the hypothesis of an underlying (VdPFN) scenario in our system.

V. NUMERICAL RESULTS

A. System parameters

In the present study we consider as free parameters the cold-cavity detuning δ_0, the injected optical power P_{in}, and the mechanical quality factor Q while the other parameters (mass, frequency, finesse…), determining the strength of the radiation-pressure effect, will be fixed at realistic values for a Fabry-Perot cavity: $m=50$ g, $\Omega=2\pi\times100$ Hz, $\lambda=1.064$ μm, $F=80\,000$, $A=40\,000$, leading to $\alpha\approx4P_{in}$ where P_{in} expressed in mW. The photothermal parameters β and ε can be experimentally determined through the characterization of the photothermal effect in the system, as described in Refs. [16,29]. On the base of these experiments, we take a time scale ratio of $\varepsilon=10^{-2}$ and $\beta=2.4P_{in}$.

For simplicity we keep the above parameters as fixed in all the numerical simulations reported in the present work. We remark, however, that the observed dynamic regimes do not depend on this particular choice of parameters. By changing the physical properties of the interferometer we can find again the same behavior in correspondence of different injected powers and/or cold-cavity detuning. The nonlinear effects here described can always be observed provided that radiation pressure and photothermal effects are sufficiently strong to change the cavity resonance by at least one half

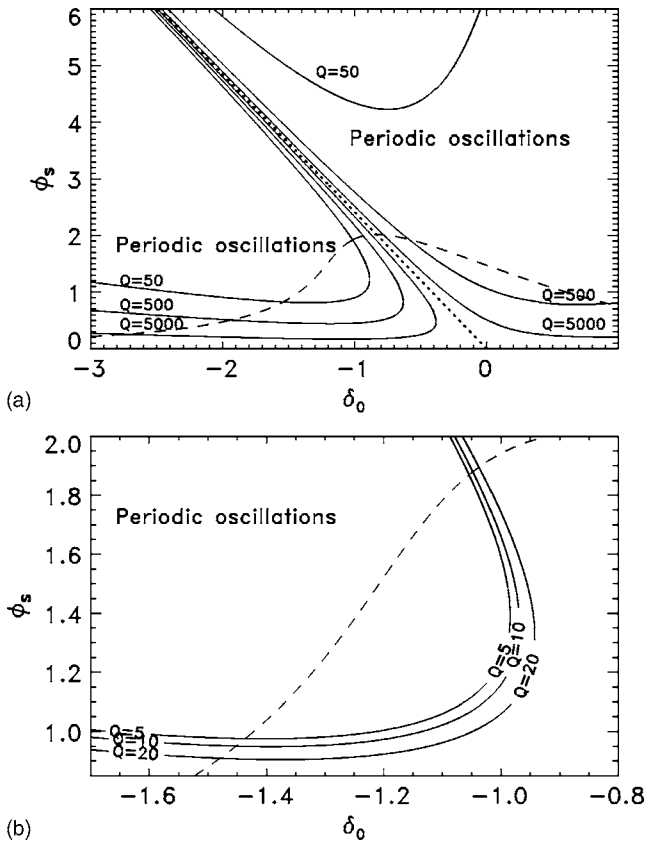

FIG. 6. (a) Hopf bifurcation boundary (solid lines) for different values of Q. The dotted line represents the curve $C=0$. (b) Enlargement of the bifurcation boundary region for the values of Q corresponding to the time series in Figs. 7 and 8. The dashed line is the stationary solution ϕ_s for an injected power of 0.5 mW. For each value of Q, the stability domain consists of a small region around the dotted line limited by the corresponding bifurcation boundary (solid lines).

linewidth Δ (i.e., α and β must be of the order of 1).

B. Overdamped system: $Q=1$

In this section we discuss the dynamic regimes of our system obtained by numerical integration of Eqs. (9a)–(9c). We first consider the overdamped case $Q=1$ and an injected power of 0.5 mW. The temporal series of the system variables ϕ and θ for different values of δ_0 are reported in Fig. 3.

Far from resonance ϕ and θ are constant in time (stable steady state). In correspondence of a critical value of δ_0, a supercritical Hopf bifurcation occurs and a quasiharmonic limit cycle develops [Fig. 3(a)]. The amplitude of the cycle depends on the distance from the bifurcation point and its frequency is given by the imaginary part of the linear eigenvalues of the stationary solution. Further increasing of δ_0 leads to an abrupt change in the amplitude and the shape of the Hopf limit cycle [Fig. 3(b)] and we observe a series of upward pulses. Likewise, the frequency of the oscillations experiences a sudden change from the Hopf value to the relaxation oscillation frequency. The corresponding phase-space trajectory partially follows the repelling part of the slow manifold [right panel of Fig. 3(b)]. For slightly higher values of δ_0 the time series of the fast variable ϕ [Fig. 3(c)] consists of a square-wave-like oscillation displaying abrupt jumps between intervals of slow dynamics with 50% duty cycle.

By further increasing δ_0 the reverse sequence is observed: oscillation of downward pulses [Fig. 3(d)], a quasiharmonic limit cycle [Fig. 3(e)] with an offset respect to that in Fig. 3(a) and finally a new stable steady state is reached.

This sequence of dynamic regimes, as well as the corresponding phase portrait projection compared to the slow manifold, are fully compatible with the transition between the two stable branches of the vdPFN model (2) as the control parameter a is varied in the interval $[-1,1]$.

Of particular interest from a dynamic point of view is a small range between the Hopf small-amplitude limit cycle and the relaxation-oscillations regime. In this parameter region, when the unstable steady state is in the neighborhoods of the fold points there are trajectories that do not jump immediatly to the other attractive branch, but follow the repelling part of the slow manifold for a certain amount of time (canard orbits). Some of these solutions are shown in Fig. 4 where the parameter δ_0 is finely varied [an example is also in Fig. 3(b)]. For higher values of δ_0, i.e., just beyond the Hopf quasiharmonic regime, the trajectories cross one of the fold points and continue moving on the slow time scale along the unstable portion of the slow manifold almost until the other fold point. As δ_0 is decreased, the amount of time spent by the system in the vicinity of the repelling part of the manifold diminishes and the orbits approach the relaxation oscillation full cycle.

Another important property of Eqs. (2) is the excitable behavior. In order to directly prove the existence of an excitable regime also in our system, we choose δ_0 such that the system is in its stable state and we apply a singular perturbation of variable amplitude $x_0\delta(t-t_0)$ to the right hand side of Eq. (8). When the amplitude x_0 is lower than a critical value, the system response is proportional to the applied stimulus (dashed and dotted traces in Fig. 5). However, for a sufficiently strong stimulus, the system recovers its stable state by following a deterministic orbit that does not depends anymore on the details of the perturbation. Note also that the trajectories in phase space clearly display the canard structure with a slow departure from the rest state in response to the applied perturbation.

In the presence of noise, unavoidable in the experiments, we have observed in our numerical simulations phenomena such as random excitable pulses, coherence resonance [30] and phase locking of the noise-induced spikes to the Hopf quasiharmonic oscillations [6]. Such effects are a straightforward consequence of the vdPFN scenario. Although their complete characterization goes beyond the purpose of the present work, their occurrence is a further confirmation of the compatibility between the vdPFN model and the dynamics of our system.

C. Dynamics for $Q>1$

In this section we present the study of the effects of a mechanical quality factor $Q>1$ on the self-oscillating re-

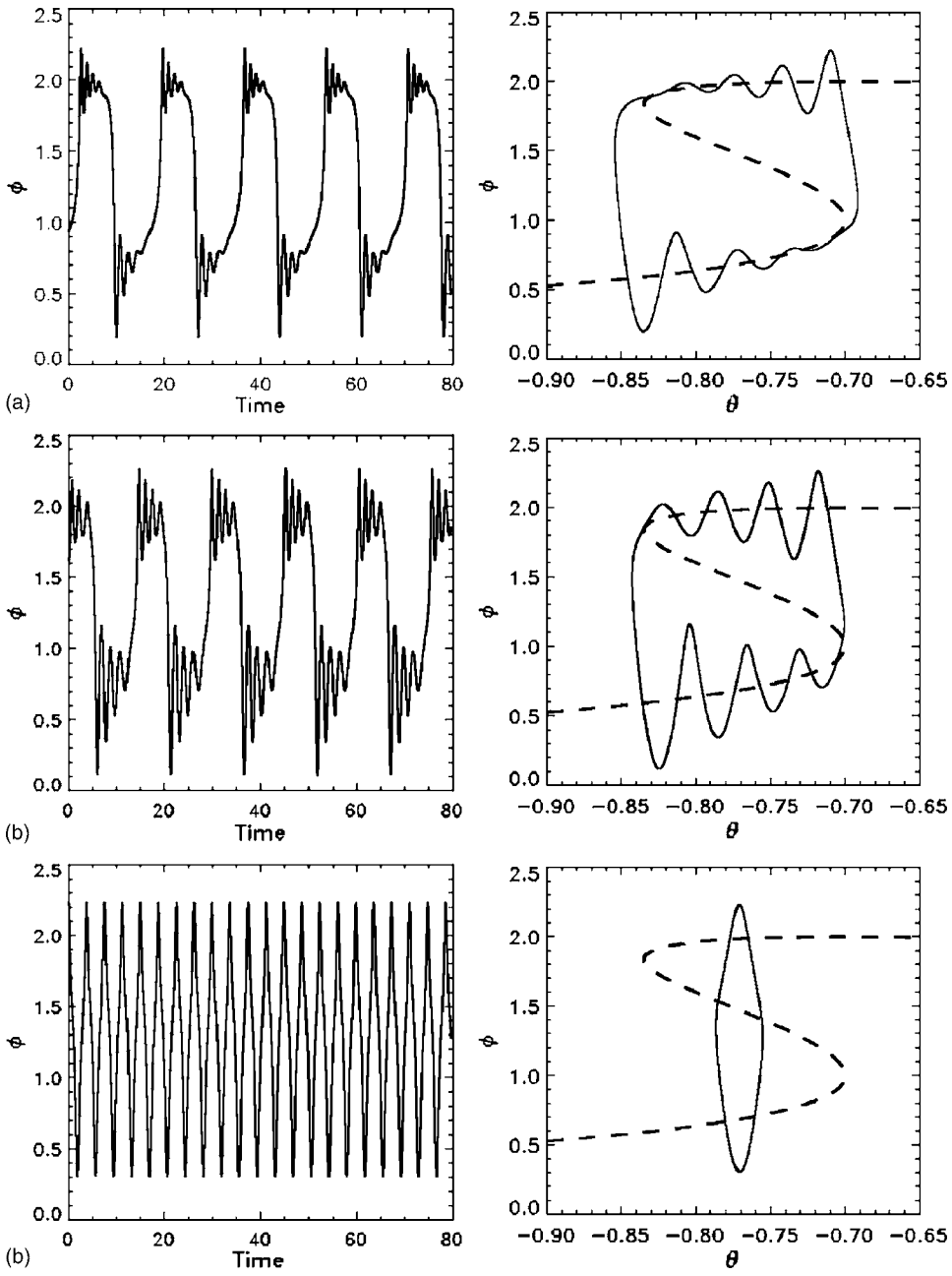

FIG. 7. Relaxation oscillations and the corresponding phase-space trajectories compared with the slow manifold (dashed line) as the parameter Q is varied: (a) $Q=5$, (b) $Q=10$, (c) $Q=20$. $\delta_0=-1.3$. The time variable is normalized to the natural period of the mechanical oscillator.

gime and on the excitable properties of our system. The question is whether the slow-fast characteristics of the relaxation oscillations can be observable also in presence of a nonoverdamped response to the forcing term αP, and how this can affect the phase-space orbits.

We first consider the limit $Q\to\infty$: in this case both the bifurcation boundary and the frequency of the Hopf limit cycle can be calculated in explicit form

$$\nu^2 = 1 + C\phi_s,$$

$$-\frac{\beta}{\alpha}C^2\phi_s^2 = 0.$$

Since $\phi_s>0$ for $P_{in}>0$ we have that $-(\beta/\alpha)C^2\phi_s^2<0$ except on the line $C=0$ where it is equal to zero. Since there is no stability change of the fixed point and the steady state solution is always unstable, the system always exhibits periodic oscillations, with a frequency which is equal to the natural frequency of the oscillator on the curve $C=0$ (if $C=0$, then $\nu^2=1$).

For finite values of Q, the Hopf bifurcation boundaries are reported in Fig. 6. We can observe [see Fig. 6(a)] that by increasing Q the oscillations region becomes larger and the bifurcation boundaries asymptotically tend to the line $C=0$, narrowing the domain in which the steady state solution is stable.

By numerical integration of our model it can be seen that Q factors of the order of few tens ($Q\approx 50$ or larger) are already sufficiently large to induce oscillations whose frequency is almost equal to Ω. In this case relaxation oscillations and excitability disappears and the only nontrivial so-

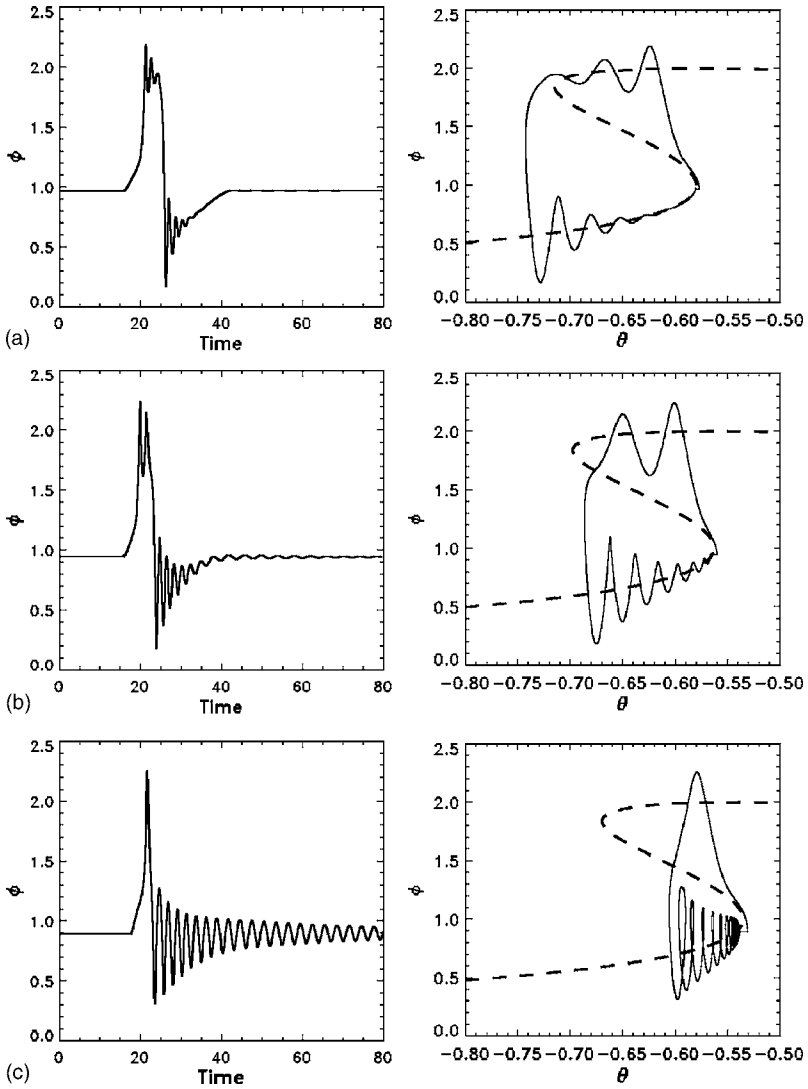

FIG. 8. Excitable response and corresponding phase space trajectories as the parameter Q is varied: (a) $Q=5$, $\delta_0=-1.420$; (b) $Q=10$, $\delta_0=-1.437$; (c) $Q=20$, $\delta_0=-1.465$. $x_0=10^{-2}$. The time variable is normalized to the natural period of the mechanical oscillator.

lutions are quasiharmonic oscillations at frequency close to Ω.

Interesting dynamics, however, can be found for intermediate values of Q, for which both the slow-fast properties and the damping term of the oscillator play a role in determining the system phase-space trajectories. For $Q=5$ [Fig. 7(a)] the temporal series exhibit relaxation oscillations, although when the system jumps from one stable branch to the other, it relaxes towards the slow attracting manifold through fast-decaying oscillations. In a small range of δ_0 values, just beyond the quasiharmonic regime, canard orbits occur. We remark that for $Q=5$ the system relaxes almost completely between one jump and the other, while for higher values of Q, the jumps occur before a complete relaxation towards the slow attracting manifold is reached [see Fig. 7(b)].

In spite of the clear differences with respect to the overdamped case, for these values of Q we can still recognize the typical phase-portrait structure of relaxation oscillations. On the other hand, for $Q=20$ [Fig. 7(c)] we cannot distinguish the slow-fast characteristics of the trajectories, whose period is already only slightly larger than $2\pi/\Omega$, although the system maintains an abrupt transition between a small amplitude limit cycle and high amplitude oscillations as well as its excitable features.

In order to characterize the excitable response for different values of the mechanical quality factor, we fix the parameter δ_0 such that the system is close to the Hopf bifurcation point for each value of Q [see Fig. 6(b)]. We then apply a singular perturbation with amplitude sufficiently high to force system to emit a pulse. In agreement with what we have observed in the self-oscillating regime, the system relaxes towards the attracting branches of the slow manifold through damped oscillations whose amplitude and decay time increases with Q. As we can see in Fig. 8, when these damped oscillations become stronger the system returns back to its rest state before reaching the fold point of the "higher" attracting branch.

D. Canards and realistic photothermal response

We now consider a more realistic model for the photothermal frequency response. As mentioned before, the behavior of a cavity undergoing photothermal effect is well described by the frequency dependent curve $G(\tilde{\omega})$. Since the implementation of such a frequency dependence in our evolution equations is rather complicated and would require a strong numerical calculation effort, we adopted an approximated

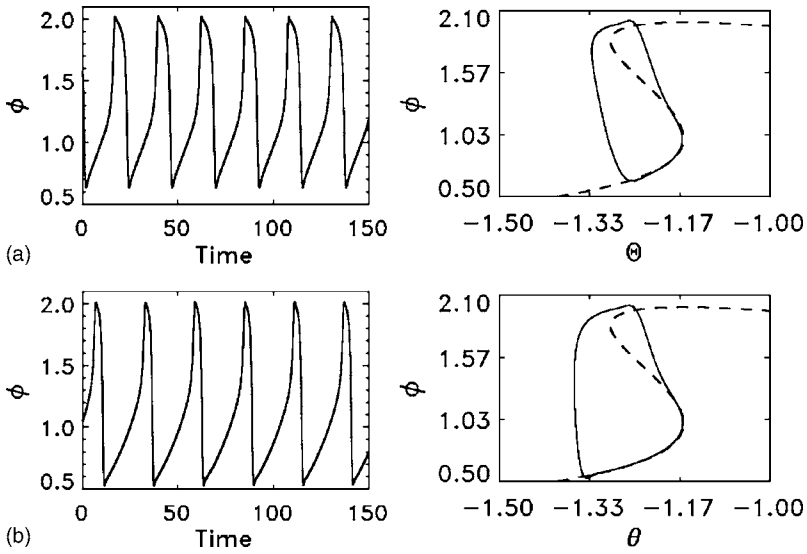

FIG. 9. Example of canard trajectories and their phase portrait projection obtained by numerical integration of (a) Eqs. (18a)–(18c) and (b) Eqs. (9a)–(9c). The time variable is normalized to the natural period of the mechanical oscillator. Parameters: (a) $N=5$, $\varepsilon_i=1.7113\times10^{-3}$, 5.0119×10^{-2}, 7.9433×10^{-1}, 5.9276, 7.9758×10^{1}; $\beta_i=9.2384\times10^{-1}$, 7.7321×10^{-1}, 4.5956×10^{-1}, 1.0016×10^{-1}, 2.8363×10^{-3}. (b) $\varepsilon=0.2\bar{\omega}_c$, $\beta=2.6\bar{B}$. $Q=1$, $\delta_0=-0.84$, $\bar{\omega}_c=0.03$, $\bar{B}=0.9$.

expression of Eq. (5) given by a sum of single-pole low-pass functions. Therefore the model reads

$$\ddot{\phi}+\frac{1}{Q}\dot{\phi}+\phi=\alpha P, \tag{18a}$$

$$\dot{\theta}_i=-\varepsilon_i\bar{\omega}_c(\theta_i+\beta_i\bar{B}P), \tag{18b}$$

$$P=\frac{1}{1+\left(\delta_0+\phi+\sum_{i=1}^{N}\theta_i\right)^2}, \tag{18c}$$

where β_i and ε_i are determined by a fitting procedure of $G(\bar{\omega})$ [31], $\bar{\omega}_c=\omega_c/\Omega$ and $\bar{B}=BAP_{in}/\Delta$.

This model, and its analysis, is more complicated than the simple single-pole approximation and we deserve its complete characterization for future studies where it will be compared directly to the experiment. However, some qualitative considerations can be expressed. We point out that the key parameters here are the time scales $\varepsilon_i\bar{\omega}_c$ and the photothermal expansion terms $\beta_i\bar{B}$. In the limit case of $\bar{\omega}_c=0$, we can plot the slow manifold $\bar{\Sigma}=[(\phi,\Theta,v)\in\{v=0\}\cap\{F(\phi,\Theta)=0\}]$ where $\Theta=\Sigma_{i=1}^{N}\theta_i$ in the (ϕ,Θ) plane and calculate its stability as in the single-pole case. Regarding the slow subsystem equations, we remark that although not all the $\varepsilon_i\bar{\omega}_c$ are small, higher ε_i are associated to lower values of β_i (i.e., $\beta_i\bar{B}\ll1$), thereby their contribution to the system dynamics is less important. In Fig. 9 we show the system time series in the canard regime, obtained by numerical simulations of Eqs. (9b) and (18a) for a fixed value of the control parameter δ_0. We have used the experimental values taken from Ref. [16] of $\omega_c=2\pi\times3$ Hz and $B=1.5\times10^{-13}$ m/W, with $P_{in}=0.5$ mW and the usual parameters for the optical cavity and the oscillator. While some differences in the shape of the pulses in Figs. 9(a) and 9(b) can be observed, the period and the amplitude of the oscillations are quite similar, provided that the photothermal parameters in the model (9a)–(9c) are readjusted to some effective values of $\varepsilon\approx0.2\bar{\omega}_c$ and $\beta\approx2.6\bar{B}$. These results indicate that the main features of the previously observed dynamic scenario are maintained: hence in order to understand such nonlinear phenomena either from a physical and dynamical point of view, the model (9a)–(9c) is useful because it gives a simple description of the physical mechanisms underlying canard orbits and excitability in our system. On the other hand, the model (18a)–(18c) can be used for a better quantitative comparison with experiments, providing important indications about the parameters regions in which interesting dynamics can be found.

VI. CONCLUSIONS AND FUTURE PERSPECTIVES

We have shown that in high-finesse Fabry-Perot cavities the competition between radiation-pressure and photothermal effects can lead to canard oscillations and excitability occurring in the vicinity of a supercritical Hopf bifurcation. The transition between the Hopf-quasi-harmonic limit cycle and canards oscillations, as well as the dynamic regimes observed in our system, appear in an order compatible with the scenario of the vdPFN model. Beyond the interest of these phenomena from a physical and dynamic point of view, their characterization in our nonlinear optical cavity is critical for experiments involving high sensitivity interferometric displacement measurements, as those necessary for gravitational waves detection.

In a different range of parameters of the mechanical oscillator, preliminary numerical studies indicate also the existence of different dynamic regimes such as mixed mode oscillations [32] and aperiodic spiking. The theoretical analysis of such dynamics as well as the experimental study of the phenomena reported in the present paper will be the subject of future works.

ACKNOWLEDGMENT

This work was partially funded by ILIAS Project No. RII3-CT-2003-506222.

[1] C. K. Jones and A. I. Khibnik, *Multiple-time-scale Dynamic Systems*, IMA Proceedings No. 122 (Springer-Verlag, New York, 2000).
[2] E. Izhikevich, Int. J. Bifurcation Chaos Appl. Sci. Eng. **10**, 1171 (2000).
[3] J. M. Davidenko *et al.*, Nature (London) **355**, 349 (1992).
[4] A. M. Zhabotinskii, *Concentration Autooscillations* (Nauka, Moscow, 1974).
[5] J. D. Murray, *Mathematical Biology* (Springer-Verlag, Berlin, 1989).
[6] V. A. Makarov, V. I. Nekorkin, and M. G. Velarde, Phys. Rev. Lett. **86**, 3431 (2001).
[7] E. I. Volkov, E. Ullner, A. A. Zaikin, and J. Kurths, Phys. Rev. E **68**, 026214 (2003).
[8] R. FitzHugh, Biophys. J. **1**, 445 (1961);J. Nagumo, S. Arimoto, and S. Yoshizawa, Proc. IRE **50**, 2061 (1962).
[9] M. W. Hirsch and S. Smale, *Differential Equations, Dynamic Systems and Linear Algebra* (Academic Press, New York, London, 1974).
[10] J. L. Callot, F. Diener, and M. Diener, C.R. Seances Acad. Sci., Ser. A **286**, 1059 (1978).
[11] M. Giudici, C. Green, G. Giacomelli, U. Nespolo, and J. R. Tredicce, Phys. Rev. E **55**, 6414 (1997).
[12] S. Barland, O. Piro, M. Giudici, J. R. Tredicce, and S. Balle, Phys. Rev. E **68**, 036209 (2003).
[13] F. Marino, G. Catalan, P. Sanchez, S. Balle, and O. Piro, Phys. Rev. Lett. **92**, 073901 (2004).
[14] E. A. Avrutin, J. H. Marsh, and J. M. Arnold, Int. J. Optoelectron. **10**, 427 (1995).
[15] B. Krauskopf *et al.*, Opt. Commun. **215**, 367 (2003).
[16] M. De Rosa, L. Conti, M. Cerdonio, M. Pinard, and F. Marin, Phys. Rev. Lett. **89**, 237402 (2002).
[17] C. Fabre *et al.*, Phys. Rev. A **49**, 1337 (1994).
[18] A. Heidmann, Y. Hadjar, and M. Pinard, Appl. Phys. B: Lasers Opt. **64**, 173 (1997).
[19] J. M. Aguirregabiria and L. Bel, Phys. Rev. A **36**, 3768 (1987).
[20] V. Chickarmane, S. V. Dhurandhar, R. Barillet, P. Hello, and J. Y. Vinet, Appl. Opt. **37**, 3236 (1998).
[21] S. V. Dhurandhar, P. Hello, B. S. Sathyaprakash, and J. Y. Vinet, Appl. Opt. **36**, 5325 (1997).
[22] A. Dorsel, J. D. McCullen, P. Meystre, E. Vignes, and H. Walther, Phys. Rev. Lett. **51**, 1550, (1983).
[23] P. Meystre, E. M. Wright, J. D. McCullen, and E. Vignes, J. Opt. Soc. Am. B **2**, 1830 (1985).
[24] K. An, B. A. Sones, C. Fang-Yen, R. R. Dasari, and M. S. Feld, Opt. Lett. **22**, 1433 (1997).
[25] M. Pinard, Y. Hadjar, and A. Heidmann, Eur. Phys. J. D **7**, 107 (1999).
[26] L. Conti *et al.*, J. Appl. Phys. **93**, 3589 (2003).
[27] V. B. Braginsky, M. L. Gorodetsky, and S. P. Vyatchanin, Phys. Lett. A **264**, 1 (1999).
[28] M. Cerdonio, L. Conti, A. Heidmann, and M. Pinard, Phys. Rev. D **63**, 082003 (2001).
[29] F. Marin *et al.*, in *Proceedings of the 6th Edoardo Amaldi Conference on Gravitational Waves, Okinawa, Japan, June 20-24, 2005*.
[30] A. S. Pikovsky and J. Kurths, Phys. Rev. Lett. **78**, 775 (1997).
[31] M. De Rosa and F. Marin (unpublished).
[32] A. Goryachev, P. Strizhak, R. Kapral, J. Chem. Phys. **107**, 2881 (1997).